European Journal of Pharmaceutics and Biopharmaceutics 141 (2019) 1–11

Contents lists available at ScienceDirect

European Journal of Pharmaceutics and Biopharmaceutics

journal homepage: www.elsevier.com/locate/ejpb

Research paper

# Near-infrared light-responsive, pramipexole-loaded biodegradable PLGA microspheres for therapeutic use in Parkinson's disease

Shuang Li, Jiaxin Liu, Ge Li, Xueyan Zhang, Fei Xu, Zhijiang Fu, Lesheng Teng, Youxin Li*, Fengying Sun*

*School of Life Sciences, Jilin University, Changchun, Jilin 130012, China*

ARTICLE INFO

*Keywords:*
Pramipexole
Parkinson's disease
Near-infrared responsive
Hollow gold nanospheres
Microspheres

ABSTRACT

Parkinson's disease (PD) is associated with symptoms such as tremor and bradykinesia which, together with a rigorous dosing regimen, can place an untenable burden on patients. These issues underscore the need for triggerable, modulated drug delivery systems. Currently, pramipexole (PRX) is the most widely used non-ergot dopamine agonist for the treatment of PD. In this study, near-infrared light-responsive PRX and hollow gold nanospheres (HGNS)-loaded biodegradable poly (D, L-lactide-co-glycolide) (PLGA) microspheres (PRX/HGNS MS) were fabricated using solid-in-oil-in-water (S/O/W) and water-in-oil-in-water (W/O/W) emulsion-solvent evaporation techniques to achieve modulated drug release. The PRX/HGNS MS were uniform, with an average diameter of approximately 24 μm, favorable PRX and HGNS encapsulation efficiencies (51.71 ± 0.54% and 65.15 ± 2.30%, respectively) and rapid, controllable drug release both *in vitro* and *in vivo*. Cytotoxicity tests revealed no significant differences between HGNS and PRX/HGNS MS when compared with a negative control. Pharmacodynamics and immunohistochemistry studies revealed a more rapid recovery of striatum in the group treated with PRX/HGNS MS produced using the S/O/W method. The results clearly demonstrate that light-responsive PRX/HGNS MS produced using the S/O/W method have the potential to address PD patients' mobility problems in a smart, controllable and remotely triggerable manner.

## 1. Introduction

Parkinson's disease (PD) is the second-most prevalent chronic and progressive neurodegenerative disorder, with nearly 2% of the global population exhibiting symptomatic disease during late middle or older age [1,2]. Pathologically, PD is mainly characterized by the selective loss of dopaminergic cells and deficiencies in striatum dopamine (DA), as well as its metabolites homovanillic acid (HVA) and 3,4-dihydroxyphenylacetic acid (DOPAC). These abnormalities lead to symptoms such as cognitive impairment, tremor, rigidity and bradykinesia [3,4].

In 1997, pramipexole (PRX), a dopamine D2 and D3 receptor agonist, was approved by the Food and Drug Administration (FDA) for the treatment of PD [5–7]. However, the efficacy of PRX is limited by its short half-life, which necessitates a frequent, rigorous, and highly inconvenient dosing schedule [8]. Such regimens, together with the symptoms of PD, place a heavy burden on patients and may lead to non-compliance with treatment. These limitations clearly underscore the need for triggerable drug delivery systems [9].

The new generation of smart drug delivery involves the use of remotely triggerable systems designed to achieve appropriate temporal and spatial control of drug release, enhance drug efficacy and decrease systemic toxicity non-invasively [10,11]. Biomedical studies have increasingly identified the potential use of near-infrared (NIR) light-responsive drug delivery systems, which have been shown to provide appropriate temporal and spatial control, a high level of convenience, on-demand drug release and dermal penetrability [12,13]. In this context, gold nanostructures, such as hollow gold nanospheres (HGNS), have been used as photosensitive materials that exhibit a strong photothermal effect due to localized surface plasmon resonance in response to NIR wavelengths (780–850 nm) [14,15].

Previously, we reported the use of biodegradable polymeric microspheres for the predetermined, sustained and local release of drugs over time [16,17]. Another study investigated the ability of gold nanostructures encapsulated in poly (D, L-lactide-co-glycolide) (PLGA) microspheres via a water-in-oil-in-water (W/O/W) emulsion-solvent evaporation method to enable the photothermal ablation of cancer cells [18]. However, the improved solid-in-oil-in-water (S/O/W) emulsion-solvent evaporation method has not previously been used to prepare

* Corresponding authors.
*E-mail addresses:* liyouxin@jlu.edu.cn (Y. Li), sunfengying@jlu.edu.cn (F. Sun).

https://doi.org/10.1016/j.ejpb.2019.05.013
Received 19 January 2019; Received in revised form 4 May 2019; Accepted 14 May 2019
Available online 14 May 2019

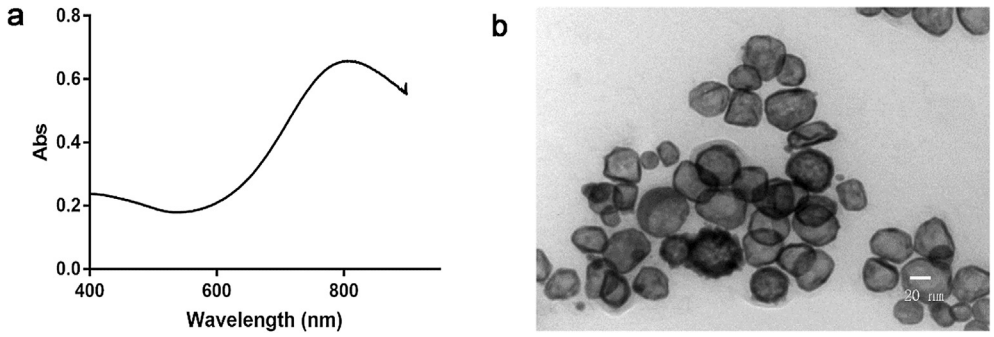


**Fig. 1.** Characterization of HGNS. (a) Absorption spectrum of HGNS at the concentration of 0.5 mg/mL. (b) TEM image of HGNS.

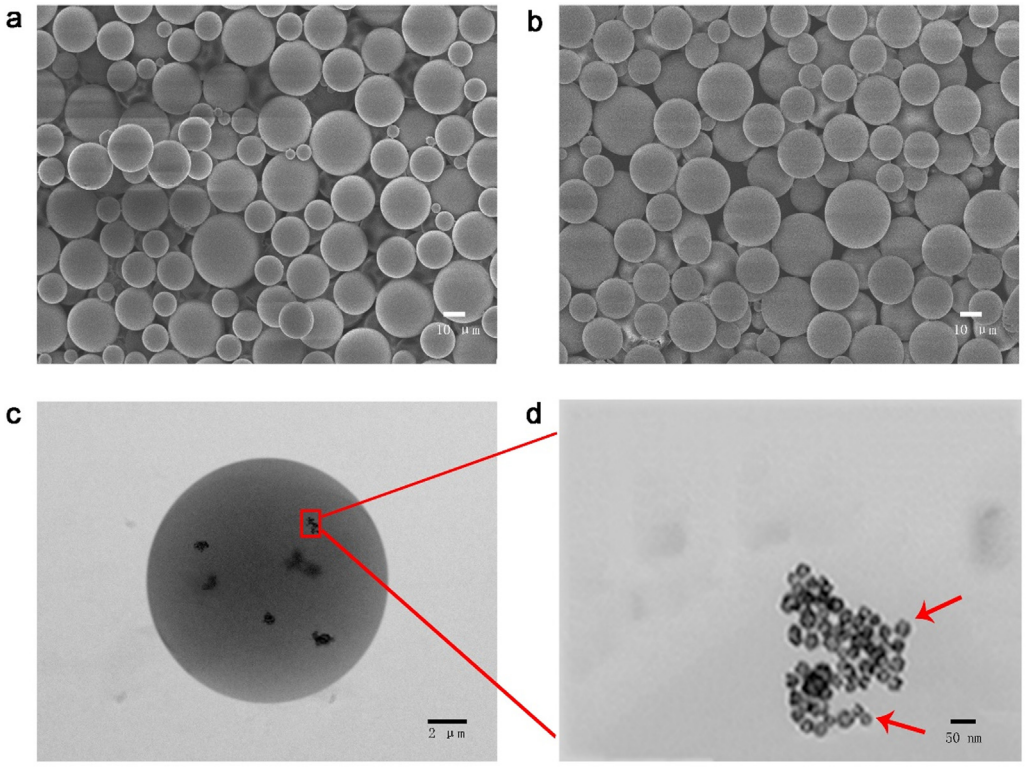


**Fig. 2.** Characterization of microspheres. SEM images of PRX/HGNS MS prepared by W/O/W method (a) and S/O/W method (b). TEM images of PRX/HGNS MS prepared by S/O/W method (c) and partial enlargement of it (d). Some of the single gold nanosphere were marked with red arrows.

**Table 1**
Formulations processing conditions and characteristics of microspheres (mean ± S.D. n = 3).

| Batch | PLGA | PLGA concentration (mg/mL) | PRX:PLGA (mg:mg) | DCM:DMSO (mL:mL) | Drug loading (%) | Encapsulation efficiency of PRX (%) |
|---|---|---|---|---|---|---|
| 1 | 5050 2A | 180 | 1:9 | 7.5:2.5 | 2.94 ± 0.07 | 29.43 ± 0.69 |
| 2 | 5050 3A | 180 | 1:9 | 7.5:2.5 | 5.17 ± 0.05 | 51.71 ± 0.54 |
| 3 | 5050 4.5A | 180 | 1:9 | 7.5:2.5 | 3.56 ± 0.08 | 35.62 ± 0.75 |
| 4 | 5050 3A | 140 | 1:9 | 7.5:2.5 | 3.21 ± 0.01 | 32.13 ± 1.21 |
| 5 | 5050 3A | 160 | 1:9 | 7.5:2.5 | 4.01 ± 0.10 | 40.11 ± 0.98 |
| 6 | 5050 3A | 180 | 1:10 | 7.5:2.5 | 4.59 ± 0.06 | 50.49 ± 0.66 |
| 7 | 5050 3A | 180 | 1:11 | 7.5:2.5 | 4.01 ± 0.09 | 48.14 ± 1.08 |
| 8 | 5050 3A | 180 | 1:9 | 7:3 | 4.97 ± 0.08 | 49.67 ± 0.78 |
| 9 | 5050 3A | 180 | 1:9 | 6:4 | 3.01 ± 0.06 | 30.12 ± 0.59 |

**Table 2**
The microspheres preparation batches of various preparation method (mean ± S.D. n = 3).

| Batch | Method | Size (d. μm) | Encapsulation efficiency of PRX (%) | Encapsulation efficiency of HGNS (%) |
|---|---|---|---|---|
| 10 | W/O/W | 23.02 ± 6.00 | 50.09 ± 0.68 | 29.23 ± 3.28 |
| 11 | S/O/W | 25.23 ± 5.10 | 51.71 ± 0.54 | 65.15 ± 2.30 |

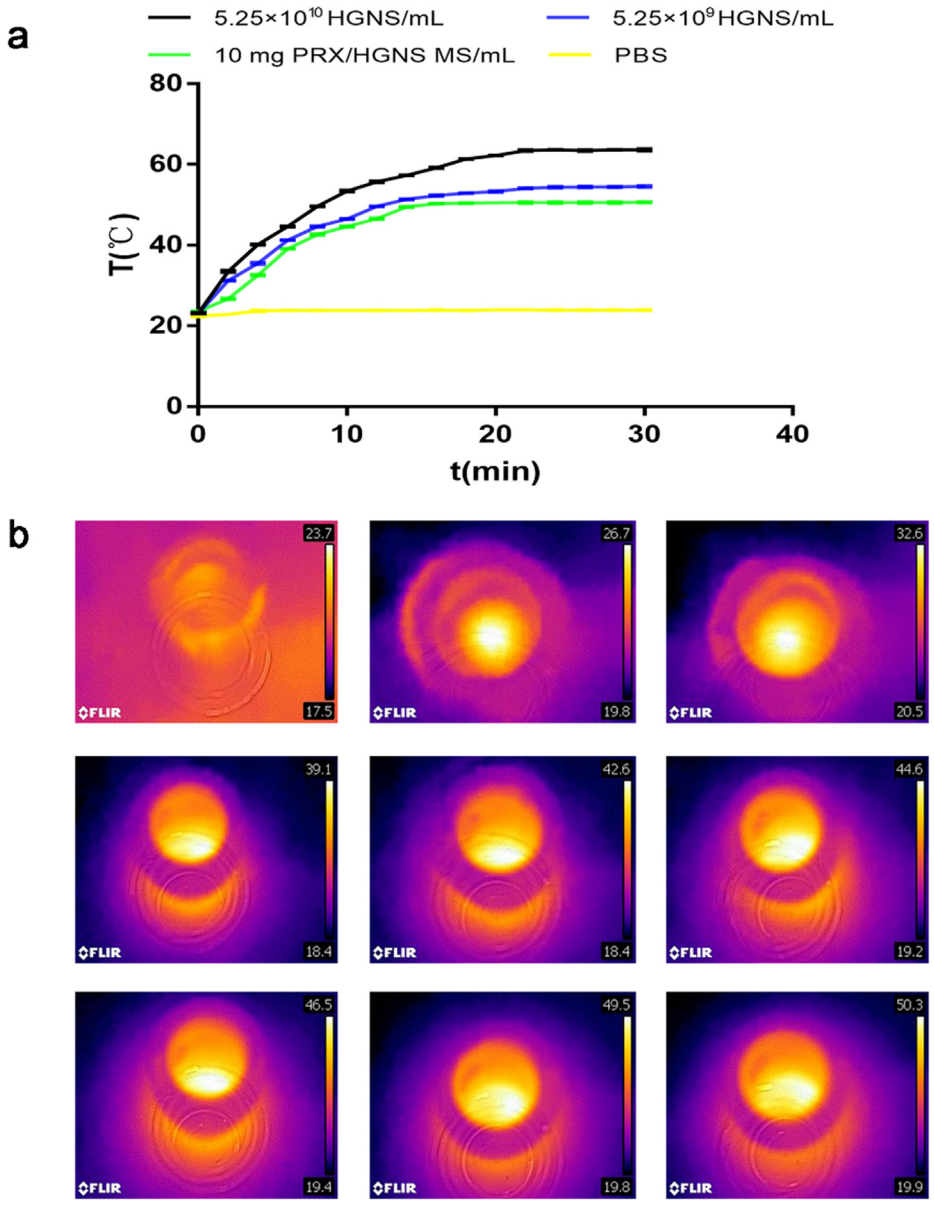


**Fig. 3.** Photothermal effect of HGNS and PRX/HGNS MS. (a) Temperature changes of PBS (pH 7.4, 10 mM), $5.25 \times 10^9$ and $5.25 \times 10^{10}$ particles/mL HGNS and 10 mg/mL PRX/HGNS MS after exposure to NIR laser at an output power of 2.55 W $cm^{-2}$. The data are expressed as the mean ± S.D. (n = 3). (b) FLIR images of PRX/HGNS MS at 2 min intervals in 16 min after exposure to NIR laser.

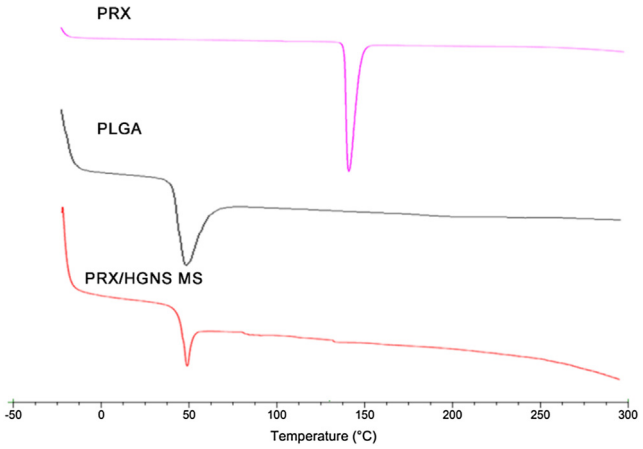


**Fig. 4.** DSC spectrum of PRX, PLGA, PRX/HGNS MS.

NIR light-responsive PLGA microspheres. Furthermore, few studies have investigated the potential of NIR light-responsive drug delivery systems as a smart, controllable and remotely triggerable option that addresses the mobility problems of patients with degenerative diseases such as PD.

In this study, we fabricated PRX and HGNS-loaded biodegradable PLGA microspheres (PRX/HGNS MS) with the aim of using NIR light to modulate the release of a model drug. HGNS were synthesized using poly (vinylpyrrolidone) $(C_6H_9NO)_n$ (PVP, $M_w$ = 55,000 Da) as a template stabilizing agent and could be lyophilized without structural damage. This enabled the use of the S/O/W emulsion-solvent evaporation method of preparation, which increased the loading efficiency of HGNS and enhanced the controllability of drug release (compared to the traditional W/O/W method). We additionally investigated the drug-release properties of PRX/HGNS MS through studies of morphology, drug loading, encapsulation efficiency, differential scanning calorimetry (DSC), *in vitro* drug release, *in vitro* cytotoxicity, pharmacokinetics, pharmacodynamics and immunohistochemistry.

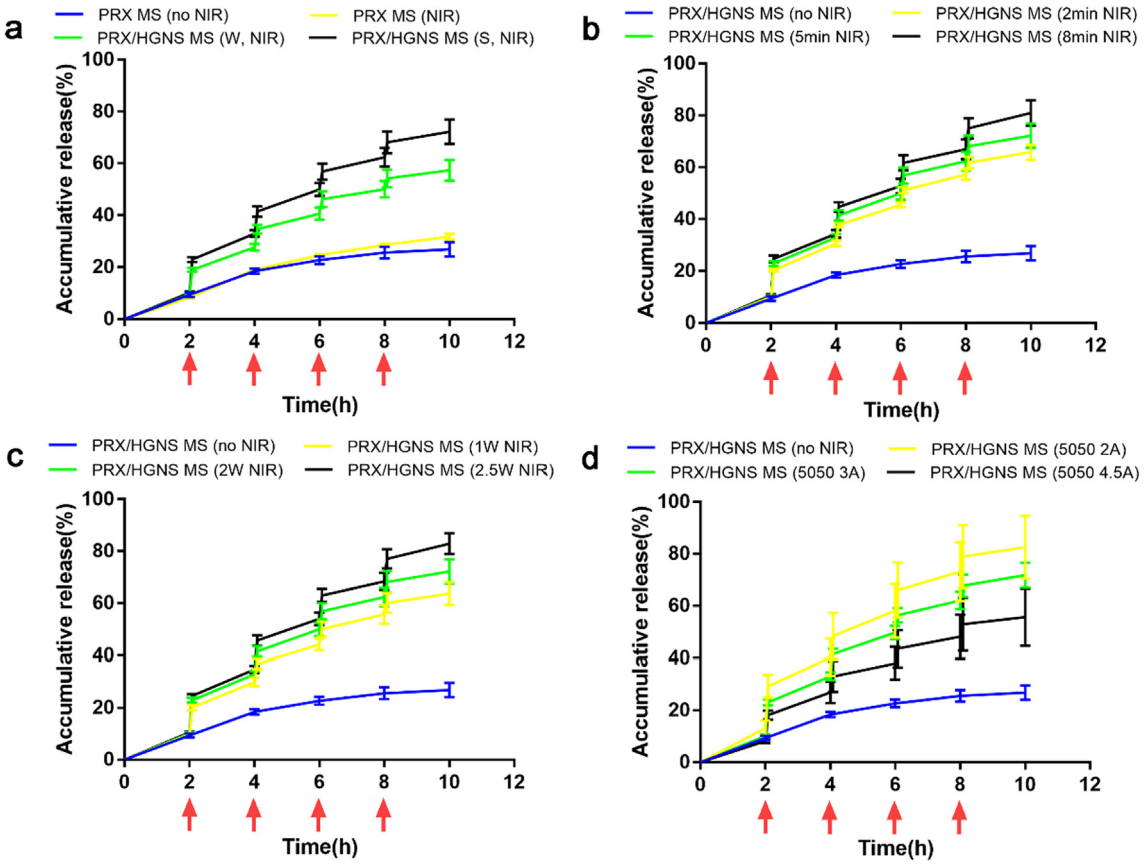


**Fig. 5.** *In vitro* release of PRX from microspheres with NIR radiation at the time points of 2 h, 4 h, 6 h, 8 h. (a) Microspheres prepared by W/O/W and S/O/W methods with or without NIR laser. (b) PRX/HGNS MS by S/O/W method irradiated with NIR laser for 2 min, 5 min, 8 min at the power of 2 W. (c) PRX/HGNS MS by S/O/W method irradiated with NIR laser for 5 min at the power of 1 W, 2 W, 2.5 W. (d) PRX/HGNS MS using S/O/W method prepared by PLGA of different viscosity irradiated with NIR laser for 5 min at the power of 2 W. The data are expressed as the mean ± S.D. (n = 3).

## 2. Materials and methods

### 2.1. Materials

PLGA polymers (5050 2A, $M_w$ = 10,000 Da) (5050 3A, $M_w$ = 29,000 Da) (5050 4.5A $M_w$ = 51,000 Da) were donated by Luye Pharmaceutical Co., Ltd. (Shandong, China). PRX (AR, > 98%) were purchased from Bide pharm. (Shanghai, China). Sodium borohydride ($NaBH_4$) and 1-methyl-4-phenyl-1, 2, 3, 6-tatrahydropyridine hydrochloride (MPTP) were purchased from Aladdin (Shanghai, China). Cobalt chloride ($CoCl_2$), polyvinyl alcohol (PVA, 87–89% hydrolyzed, $M_w$ = 13,000–23,000 Da) were purchased from Sigma-Aldrich (St. Louis, MO, USA). Chloroauric acid trihydrate ($HAuCl_4{\cdot}3H_2O$), PVP, 3-(4,5-dimethylthiazol-2-yl)-2,5-diphenyl tetrazolium bromide (MTT) were purchased from Yuanye Biotech Co., Ltd. (Shanghai, China). Anti-tyrosine hydroxylase antibody (TH) and horseradish peroxidase-conjugated antibodies were obtained from Cell Signaling Technology Inc. (Boston, USA). All cell culture media and supplements were obtained from Thermo Fisher Scientific (Waltham, MA, USA). Remaining reagents were of analytical grade. All experiments used ultrapure water.

### 2.2. Synthesis and characterization of HGNS

HGNS were synthesized via a galvanic exchange [19,20]. A three-necked round-bottom flask was filled with 200 mL of deoxygenating deionized water containing 0.08 mmol sodium citrate, 0.12 mmol $CoCl_2$ and 0.2 mmol PVP. A constant flow of argon gas was pumped into this solution for 60 min. Subsequently, 500 μL of 0.6 mol $NaBH_4$ aqueous solution prepared by fresh ice-cold water was injected immediately into the flask while stirring at a speed of 500 rpm using a magnetic stirrer (KIKA, German). The mixture was stirred continuously until the color changed from pale pink to either gray or brown, which confirmed the synthesis of the $Co_2B$ nanoparticles scaffold. Subsequently, 5 mL of a freshly prepared solution containing 0.003 mol $HAuCl_4{\cdot}3H_2O$ was injected into the flask, and the solution was reacted for another 30 min under argon gas flow and continuous stirring. Subsequently, the solution was exposed to air until the color changed to dark green, indicating the complete oxidation of cobalt and formation of hollow gold spheres. The reaction products were collected by centrifugation at 14,000 rpm and 20 °C for 20 min and washed three times with an aqueous solution containing 0.1% PVP. The final products were suspended and lyophilized using an ALPHA 1-2LD PLUS lyophilizer (Christ, Osterode am Harz, Germany) for 18 h.

Ultraviolet (UV)-visible absorption measurements were performed on a UV–visible spectroscope (SHIMADZU, Japan) with a spectral resolution of 0.5 nm. To determine the morphology, the average shell thickness and diameter of the HGNS were examined using an H-800 transmission electron microscope (TEM) (Hitachi, Japan).

### 2.3. Preparation of PRX/HGNS MS using the S/O/W and W/O/W methods

PRX/HGNS MS were first prepared using the S/O/W double emulsion-solvent evaporation method. The oil phase comprised different ratios of DCM containing PLGA and DMSO containing PRX (total weight of PLGA and PRX = 200 mg, total volume of dichloromethane and DMSO = 1 mL). The freeze-dried HGNS were emulsified in this oil phase for 60 s at low temperature (ice bath), using an ultrasonic processor at 4 W (SCIEMTZ, China). The stabilized suspension was then

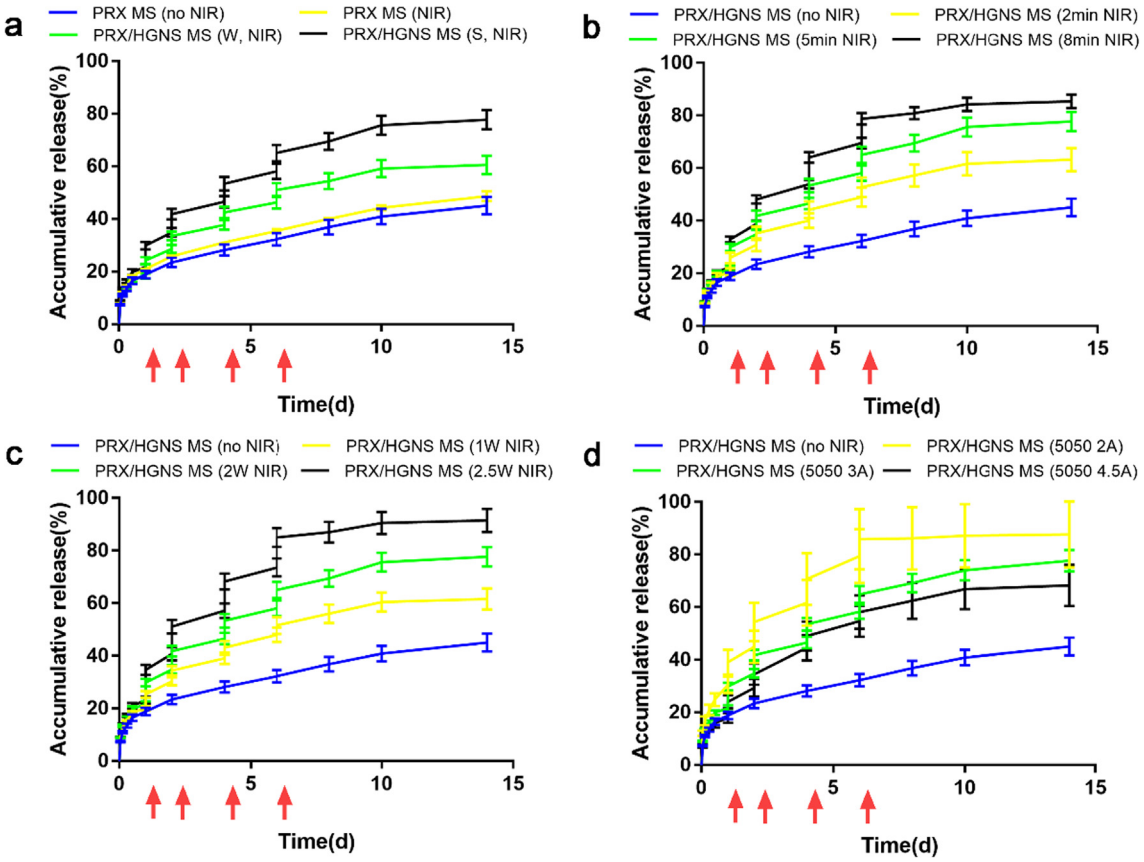


**Fig. 6.** *In vitro* release of PRX from PLGA microspheres with NIR radiation at the time points of 1 d, 2 d, 4 d, 6 d. (a) Microspheres prepared by W/O/W and S/O/W methods with or without NIR laser. (b) PRX/HGNS MS by S/O/W method irradiated with NIR laser for 2 min, 5 min, 8 min at the power of 2 W. (c) PRX/HGNS MS by S/O/W method irradiated with NIR laser for 5 min at the power of 1 W, 2 W, 2.5 W. (d) PRX/HGNS MS using S/O/W method prepared by PLGA of different viscosity irradiated with NIR laser for 5 min at the power of 2 W. The data are expressed as the mean ± S.D. (n = 3).

slowly injected into 5 mL of 1% (w/v) PVA and subsequently homogenized for 2 min on ice using a homogenizer at 4000 rpm. The resulting emulsion was immediately poured into 100 mL of 0.1% (w/v) PVA and allowed to solidify into microspheres under gentle magnetic stirring for a minimum of 3 h. The resulting microspheres were washed three times with distilled water via centrifugation at 10,000 rpm and 4 °C for 10 min, and suspended uniformly in an appropriate volume of distilled water. The microspheres were subsequently lyophilized and stored at 4 °C for further analysis.

For comparison, PRX/HGNS MS were also prepared using the W/O/W emulsion-solvent evaporation method with the same oil phase. The HGNS suspension was emulsified in the oil phase for 60 s at a low temperature (ice bath) using an ultrasonic processor at 4 W. The remaining steps were performed as described for the S/O/W emulsion-solvent evaporation method.

### 2.4. Morphological analysis

The surface morphology and appearance of the PRX/HGNS MS were evaluated and imaged using a JXA-840 scanning electron microscope (SEM) (JEOL, Japan). For this analysis, microspheres suspension at a concentration of 1 mg/mL were loaded on the surfaces of specimen stubs and vacuum-coated with gold film at an accelerating voltage of 3 kV. Subsequently, the samples were ultrasonically re-suspended in distilled water and dropped into a copper grid. The surface liquid was evaporated thoroughly, and the internal morphologies of the microspheres were then investigated by TEM at an acceleration voltage of 200 kV. The particle sizes of the microspheres were determined using a laser scattering particle size analyzer (Beckman Coulter, USA).

### 2.5. Drug loading and encapsulation efficiencies of PRX and HGNS

The drug loading and encapsulation efficiency of PRX were detected via high-performance liquid chromatography (HPLC) (Waters, USA). A standard curve was generated using a range of PRX standard concentrations (0–500 μg/mL), which yielded a high correlation coefficient ($R^2$ = 0.9999). Next, 10 mg of microspheres were dissolved in 1 mL of acetonitrile and subsequently diluted to 10 mL in the mobile phase, which comprised a 0.35% ammonium acetate solution, methanol and acetonitrile at a ratio of 75:16:9 (v/v). The concentration of this solution was measured by UV detection with an absorption peak at 252 nm. An Agilent Extend C18 column (4.6 mm × 250 mm, 5 μm; Agilent Technologies, Inc., USA) was used for drug separation. The injection volume, column temperature and flow rate were set at 20 μL, 30 °C and 1 mL/min, respectively. Actual drug loading was calculated as the ratio of the weight of PRX encapsulated in the microspheres to the total weight of the microspheres. Encapsulation efficiency was calculated as the ratio of the actual weight of encapsulated PRX to the theoretical loading of PRX.

The encapsulation efficiency of HGNS was calculated by measuring the UV–visible absorbance of the microspheres at 808 nm. First, 10 mg of microspheres were first dissolved in an appropriate volume of dichloromethane and then extracted using 5 mL of distilled water. A calibration curve was fabricated using known gradient concentrations of HGNS diluted in aqueous solution. The calibration values were calculated at an absorbance at 808 nm and extinction coefficient of $\varepsilon = 8.3 \times 10^9\,\mathrm{L\,mol^{-1}\,cm^{-1}}$ ($1.37 \times 10^{-11}\,\mathrm{mL\,particle^{-1}\,cm^{-1}}$).

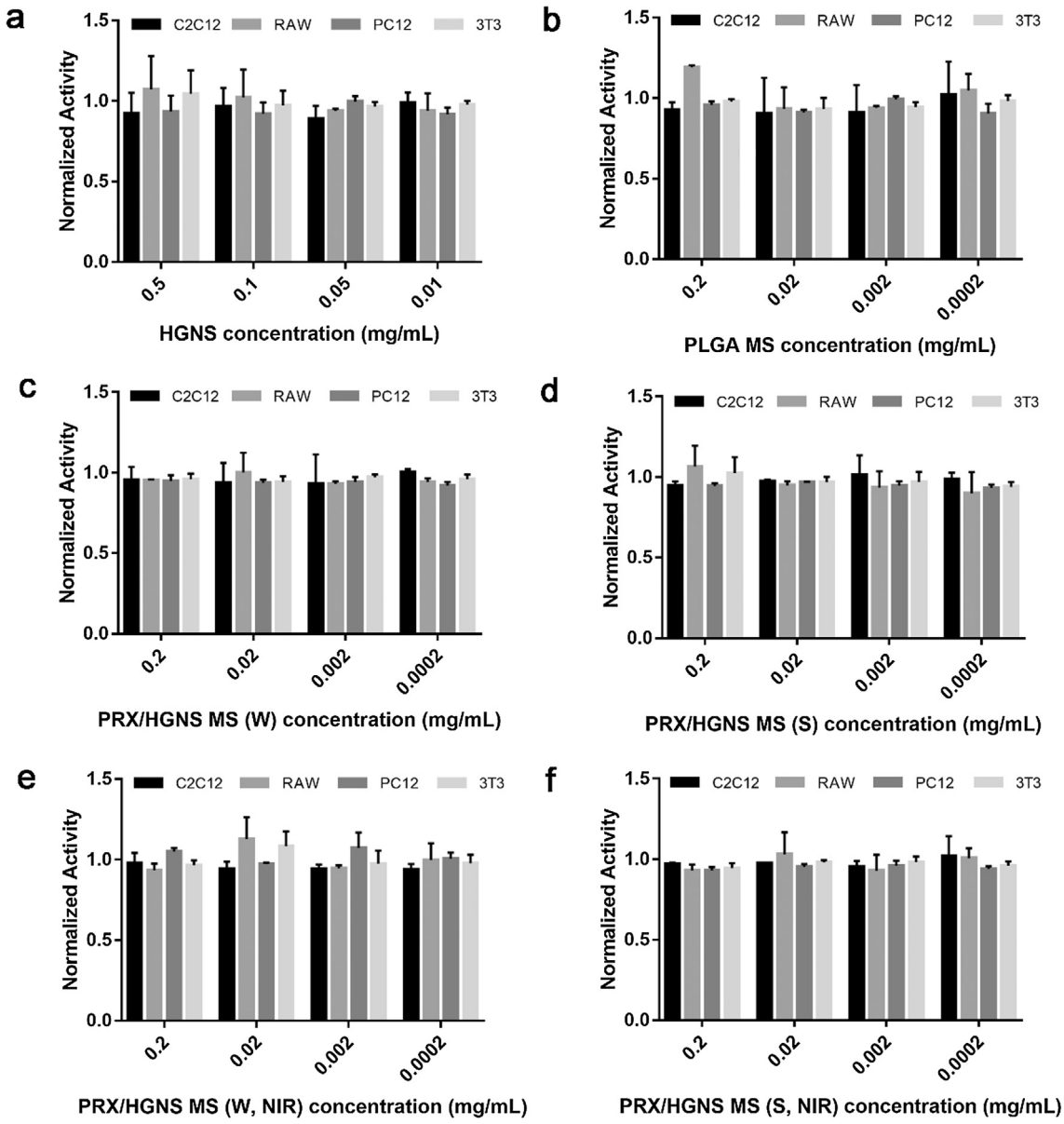


**Fig. 7.** Cytotoxicity in the absence and presence of NIR laser. (a) Cytotoxicity of HGNS at the concentration of 0.01–0.5 mg/mL. Cytotoxicity of PLGA MS (b), PRX/HGNS MS by W/O/W method (c), PRX/HGNS MS by S/O/W method (d) at the concentration of 0.0002–0.2 mg/mL. Cytotoxicity of PRX/HGNS MS by W/O/W method (e) and S/O/W method (f) irradiated four times with NIR laser at an output power of 1 W (2 min duration each time, 2 h intervals between each irradiation) at the concentration of 0.0002–0.2 mg/mL. The data are expressed as the mean ± S.D. (n = 12).

### 2.6. The photothermal effect of HGNS and microspheres

The 808 nm NIR laser light was delivered to a penicillin bottle containing $5.25 \times 10^9$ particles/mL HGNS, $5.25 \times 10^{10}$ particles/mL HGNS or 10 mg/mL PRX/HGNS MS. A continuous wave, MDL-III-808 nm-2.5 W fiber-coupled diode NIR laser (Changchun New Industries Optoelectronics Tech. Co., Changchun, China) was used, and a 1 m, 400 μm core SMA-905 optical fiber was used to transfer the NIR laser from the laser unit to the target. The output of this fiber contained a collimator that could vary the laser spot size by changing the distance from the output to the target. An output power of 2 W yielded a spot diameter of 1 cm at a distance of 10 cm (2.55 W $cm^{-2}$). Changes in the surface temperatures of the samples were measured using infrared thermography (FLIR) at 2 min intervals over a period of 30 min. Phosphate-buffered saline (PBS) (pH 7.4, 10 mM) was used as a control.

### 2.7. DSC of microspheres

A DSC (Mettler Toledo, Zürich, Switzerland) analysis was used for the thermal characterization of PRX/HGNS MS. Approximately 5 mg of PRX, PLGA or PRX/HGNS MS were placed in an aluminum chamber and heated from −50 to 300 °C at a heating rate of 20 °C/min in a nitrogen atmosphere [8].

### 2.8. In vitro analysis of NIR-light-triggered release of PRX from microspheres

The NIR-light-triggered drug release experiments comprised two parts: one was that NIR light irradiated at the time points of 2 h, 4 h, 6 h, 8 h, the other's NIR light irradiated at 1 d, 2 d, 4 d, 6 d. The ability of NIR-light to trigger drug release was investigated as follows. First, 20 mg of microspheres per batch were suspended in 4 mL of PBS (pH 7.4, 10 mM) containing 0.1% Tween-20 (w/v) in centrifuge tubes. All

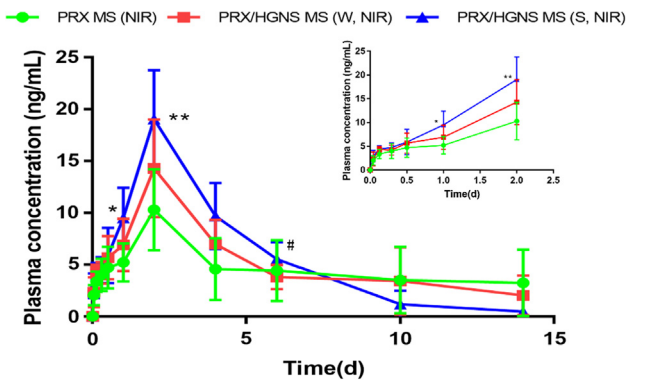


**Fig. 8.** Pharmacokinetic results of PRX MS, PRX/HGNS MS by W/O/W and S/O/W methods with NIR laser. *p < 0.5, **p < 0.01 compared to PRX MS group. #p < 0.05 compared to the group of PRX/HGNS MS by W/O/W. The data are expressed as the mean ± S.D. (n = 6).

centrifuge tubes were incubated in an orbital shaking incubator (ZHSY Inc., China) at 37 ± 1 °C and 100 rpm. At predetermined time points, a laser collimator (spot diameter: 1 cm) was fixed 10 cm from the bottom of the centrifuge tubes. The microspheres were then irradiated with 808-nm NIR light for different durations (range: 2–8 min) and powers (range: 0–2.5 W). At predetermined time intervals, the samples were then centrifuged at 8000 rpm for 8 min, and 1 mL aliquot of supernatant from each tube was collected for HPLC quantification. Each aliquot was replaced with an equal volume of fresh PBS with Tween-20. All release tests were performed in triplicate.

### 2.9. Cytotoxicity assessment

The toxicities of free HGNS and PRX/HGNS MS against cultured C2C12 myotubes, RAW macrophages, PC12 model neurons and 3T3 fibroblasts were assessed using MTT assay. All cells were obtained from the American Type Culture Collection (ATCC, USA) and seeded into 96-well plates in 100 μL of Dulbecco's Modified Eagle's Medium (DMEM) containing 10% fetal bovine serum (FBS) at a density of $1.0 \times 10^5$ cells/well. The plates were incubated in an atmosphere of 5% $CO_2$ at 37 °C. After 24 h incubation, free HGNS (0.01–0.5 mg/mL), blank PLGA microspheres (PLGA MS; 0.0002–0.2 mg/mL) or PRX/HGNS MS prepared via the W/O/W and S/O/W methods (0.0002–0.2 mg/mL) were added to the wells.

Additionally, other groups of wells containing different types of microspheres were subjected to four times of 1 W NIR laser irradiation (2 min each time separated by 2 h intervals) with a spot diameter of 1 cm. After 48 h treatment period, 20 μL of MTT solution (5 mg/mL) was added to each well, and the plates were incubated for another 4 h. Subsequently, the residual liquid was discarded from the plates, and 150 μL of DMSO was added to each well to dissolve any formazan crystals. The absorbance of each well at 490 nm was determined using a microplate reader (Perlong, China), and the relative cells viability in each well was calculated as the ratio of absorbance to that of the untreated control wells.

### 2.10. In vivo animal studies

#### 2.10.1. Animals

Sprague-Dawley (SD) rats (male, 6–8 weeks old, 180–200 g body weight) and C57BL/6 mice (male, 8 weeks old, 22–25 g body weight) were procured from the Experimental Animal Ethics Committee at the School of Life Sciences, Jilin University. All animal experiments were conducted according to the Guidelines on Humane Treatment of Lab Animals of Jilin University.

#### 2.10.2. Pharmacokinetics study

After 7 days acclimatization period, SD rats were randomly divided into the following four groups (n ≥ 6 rats per group): group 1, controls treated with intramuscular (i.m.) injections of physiological saline; group 2, i.m. injections of PRX-loaded PLGA microspheres (PRX MS) with NIR laser irradiation; group 3, i.m. injections of PRX/HGNS MS prepared by W/O/W with NIR laser irradiation; group 4, i.m. injections of PRX/HGNS MS prepared by S/O/W with NIR laser irradiation. Rats in groups 2–4 received a drug dose of 0.47 mg/kg with NIR laser irradiation at a power of 2 W for 2 min on days 1, 2, 4 and 6 (four treatments per rat). At predetermined intervals (1, 3, 7 and 12 h, 1, 2, 4, 6, 10 and 14 d) after drug administration, blood samples were collected via the retro-orbital vein into heparinized tubes. The plasma was immediately separated by centrifugation at 10,000 rpm for 10 min, and the plasma concentration of PRX was determined using HPLC [21].

#### 2.10.3. Pharmacodynamics study

After 7 days acclimatization period, C57BL/6 mice were randomly divided into the following five groups (n ≥ 6 mice per group): group 1, controls treated with intraperitoneal (i.p.) and i.m. injections of physiological saline; group 2, model animals treated with i.p. injections of MPTP and i.m. injections of PLGA MS without NIR laser irradiation; group 3, test animals treated with i.p. injections of MPTP and i.m. injections of PRX/HGNS MS without NIR laser irradiation; group 4, test animals treated with i.p. injections of MPTP and i.m. injections of PRX/HGNS MS prepared by W/O/W with NIR laser irradiation; group 5, test animals treated with i.p. injections of MPTP and i.m. injections of PRX/HGNS MS prepared by S/O/W with NIR laser irradiation.

First, the MPTP (dopaminergic neurotoxin) solution was prepared in saline and injected (i.p.) three times at 2 h intervals to yield a total dose of 40 mg/kg body weight to generate PD models on group 2, 3, 4, 5, meanwhile, mice of group 1 were injected (i.p.) physiological saline. After 24 h, mice of group 2, 3, 4, 5 received a drug dose of 0.68 mg/kg use i.m. injections, mice of group 1 were injected (i.m.) physiological saline at the same time. Then, NIR laser was irradiated at a power of 1 W for 2 min on days 1, 2, 4 and 6 after administration of microspheres (or physiological saline). The body weight of each mouse was recorded daily after the initial drug administration to evaluate acute toxicity.

Mice were subjected to a rotarod test daily after the initial drug administration to assess sensorimotor coordination and balance abilities. Each mouse was placed in a separate compartment on the rod (diameter, 0.5 cm; height, 50 cm) and tested at a speed of 25 rpm with a cut off period of 5 min. The latency of fall from the rod was calculated automatically. The behavioral test was conducted before and after

**Table 3**
Pharmacokinetic parameters of PRX/HGNS MS by W/O/W and S/O/W methods with or without NIR laser. (mean ± S.D. n = 6).

| Parameters | PRX MS | PRX/HGNS MS (W) | PRX/HGNS MS (S) |
|---|---|---|---|
| $AUC_{0\text{-}t}$ (ng h $mL^{-1}$) | 1178.58 ± 227.94 | 1666.23 ± 273.22 | 2229.59 ± 261.16 |
| $AUC_{0\text{-}\infty}$ (ng h $mL^{-1}$) | 1606.71 ± 858.95 | 1763.64 ± 251.04 | 2482.04 ± 415.30 |
| $C_{max}$ (ng/mL) | 10.31 ± 3.92 | 14.55 ± 4.39 | 19.06 ± 4.73 |
| $T_{max}$ (h) | 44.00 ± 9.80 | 44.00 ± 9.80 | 48.00 ± 0.25 |
| $T_{1/2}$ (h) | 130.31 ± 93.85 | 69.53 ± 38.34 | 90.47 ± 50.25 |
| $MRT_{0\text{-}t}$ (h) | 109.99 ± 11.96 | 111.65 ± 8.99 | 112.91 ± 15.67 |
| $MRT_{0\text{-}\infty}$ (h) | 206.57 ± 143.36 | 132.25 ± 36.46 | 150.24 ± 58.24 |

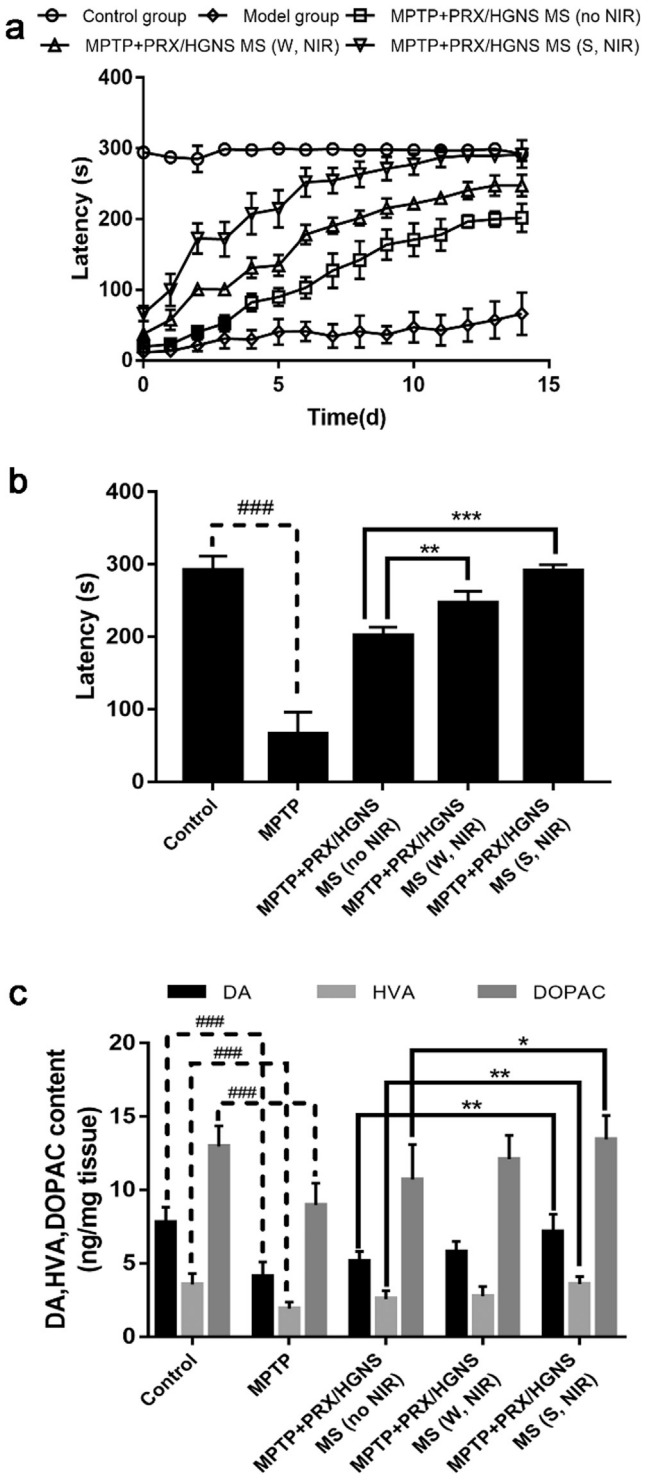


**Fig. 9.** Effects on behavioral manifestations of MPTP and PRX/HGNS MS treated mice with or without NIR laser. (a) The latency curve of mice on the rod for 14 days in the group of control, model, MPTP and PRX/HGNS MS, MPTP and PRX/HGNS MS by W/O/W and S/O/W methods with NIR laser. Solid points represent no significant difference compared to the model group. (b) The latency curve of mice on the rod in the group of control, model, MPTP and PRX/HGNS MS, MPTP and PRX/HGNS MS by W/O/W and S/O/W methods with NIR laser after 14 d. (c) The levels of DA and its metabolites (HVA and DOPAC) in the striatum in the group of control, model, MPTP and PRX/HGNS MS, MPTP and PRX/HGNS MS by W/O/W and S/O/W methods with NIR laser. *$p < 0.5$, **$p < 0.01$, ***$p < 0.001$ compared to the group of PRX/HGNS MS without NIR laser. ###$p < 0.001$ compared to the control group. The data are expressed as the mean ± S.D. (n = 6).

MPTP administration to monitor the progression of modeling.

At the end of the experiment, the mice were sacrificed. The striatum was separated from each brain, homogenized in physiological saline and centrifuged at 14,000 g for 20 min. The supernatant was filtered through 0.22 μm filter and subjected to enzyme-linked immunosorbent assay (ELISA) to quantitatively measure the concentrations of DA and its metabolites (HVA and DOPAC), which are reported as ng/mg tissue weight.

#### 2.10.4. Immunohistochemistry

Brains of mice were collected, post-fixed in 4% paraformaldehyde (PFA) for 24 h and embedded into paraffin. Three-micrometer-thick coronal sections were cut and mounted on coated slides. Slices of striatum were first rehydrated in a gradient series of xylenes and ethanol, incubated in 3% hydrogen peroxide ($H_2O_2$) for 10 min to eliminate endogenous peroxidase activity and washed five times in PBS. Subsequently, the slides were incubated with goat immune serum for 15 min, followed by an anti-tyrosine hydroxylase antibody (TH, 1/200, rabbit) for 24 h at 4 °C. The slides were subsequently washed with PBS, incubated with a biotinylated secondary antibody (1/200, goat) for 10 min at 37 °C and rinsed three times. Finally, the slides were stained with 3,3′-diaminobenzidine (DAB) for 5 min and counterstained with hematoxylin. The sections were imaged using a light microscope (Nikon Instruments Inc., Tokyo, Japan). The optical density of $TH^+$ in the striatum slides was analyzed using Motic Images Advanced 3.2 software.

### 2.11. Statistical analysis

All data are expressed as means ± standard deviations (S.D.). A one-way analysis of variance followed by the *t*-test was applied to all statistical comparisons. A p value $< 0.05$ was considered to indicate a significant difference.

## 3. Results and discussion

### 3.1. Synthesis and characterization of HGNS

To synthesize HGNS, chloroauric acid was subjected to cobalt nanoparticle-mediated reduction with PVP as a template-stabilizing agent. The absorption spectrum of HGNS included a surface plasmon resonance peak in the NIR region at 808 nm (Fig. 1a). After lyophilization, a TEM analysis of HGNS morphology revealed a near-spherical shape and uniform size distribution without apparent aggregation (Fig. 1b). Specifically, the mean diameter and gold shell thickness of prepared HGNS were 40 nm and 4 nm, respectively.

### 3.2. Synthesis and characterization of PRX/HGNS MS

PRX/HGNS MS were prepared via the W/O/W and S/O/W methods, both of which yielded microspheres with a dense texture, smooth surface and uniform sphere morphology according to scanning electron microscopy (Fig. 2a and b). TEM images revealed even dispersal of the HGNS in the matrix (Fig. 2c and d), and the latter is part of the enlargement of the former. Slight deformation of the microspheres was attributed to the thermal effect of the light source during microscopic imaging.

Next, the drug loading and encapsulation efficiency were assessed to optimize the formulation parameters. The encapsulation efficiency was found to depend on various processing conditions, including the intrinsic viscosity, polymer concentration, drug concentration and ratios of different solvents in the oil phase (Table 1). Here, PLGA 5050 3A microspheres yielded the highest PRX encapsulation efficiency of the microspheres composed of different types of PLGA, 51.71 ± 0.54%. This encapsulation efficiency increased significantly when the concentration of PLGA increased from 140 to 180 mg/mL, as the increased

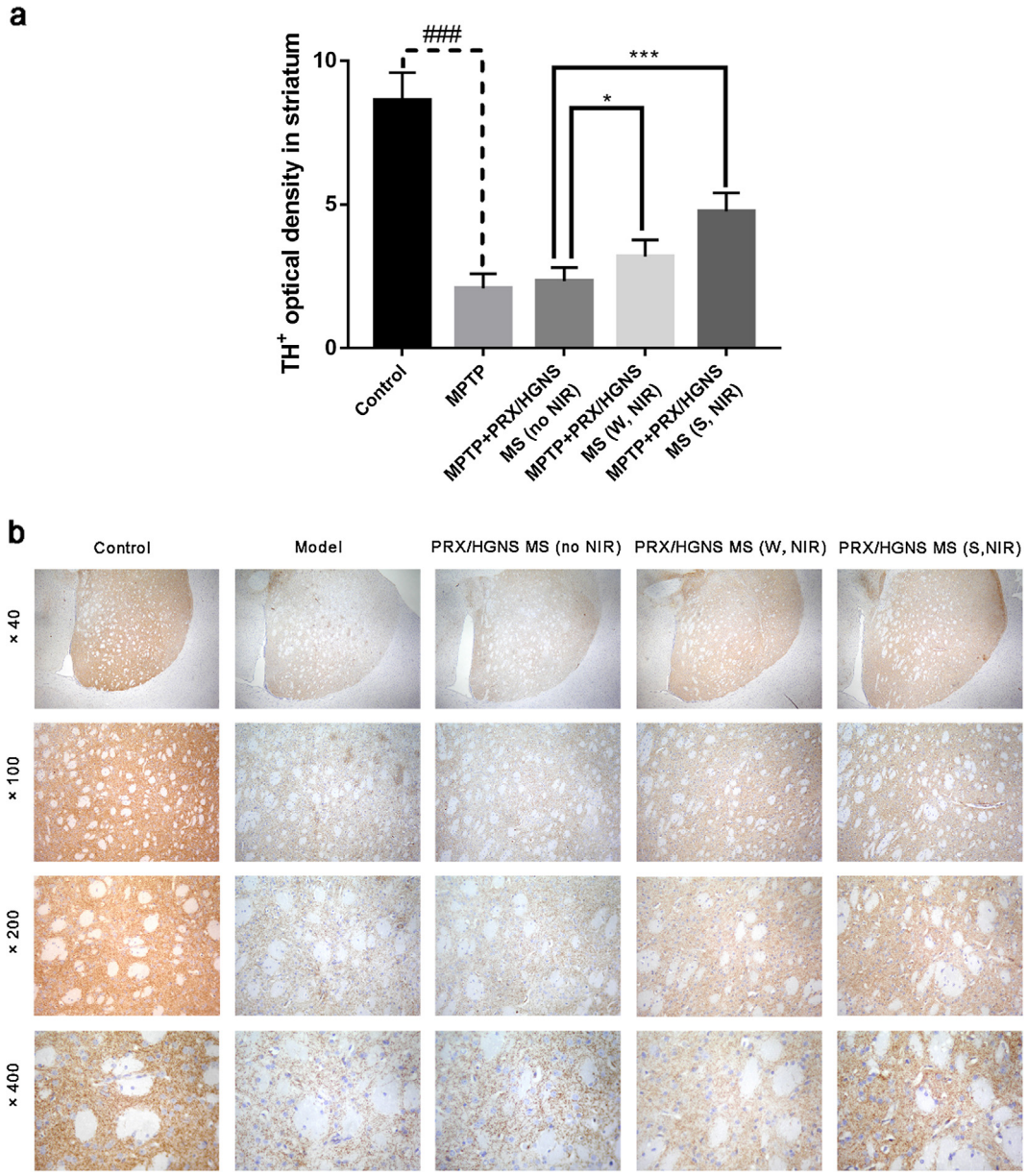


**Fig. 10.** Immunohistochemical results of MPTP and PRX/HGNS MS treated mice with or without NIR laser. (a) Striatum $TH^+$ optical density of mice in the groups of control, model, MPTP and PRX/HGNS MS, MPTP and PRX/HGNS MS by W/O/W and S/O/W methods with NIR laser after 14 d. *$p < 0.5$, ***$p < 0.001$ compared to the group of PRX/HGNS MS without NIR laser. ###$p < 0.001$ compared to the control group. The data are expressed as the mean ± S.D. (b) Striatum $TH^+$ immunohistochemical staining images of mice at 40×, 100×, 200×, 400 × magnification in the group of control, model, MPTP and PRX/HGNS MS without NIR, MPTP and PRX/HGNS MS by W/O/W and S/O/W methods with NIR laser after 14 d.

viscosity in the oil phase prevented the diffusion of PRX. The encapsulation efficiency was enhanced as the ratio of PRX:PLGA increased from 1:11 to 1:9 and the ratio of DCM:DMSO in the oil phase increased from 6:4 to 7.5:2.5, which might be explained that the solubility of PRX was higher.

The formulation was further optimized to obtain microspheres with a high HGNS encapsulation efficiency by preparing microspheres using different emulsion-solvent evaporation methods (Table 2). The HGNS encapsulation efficiency increased significantly from 29.23 ± 3.28% with the W/O/W method to 65.15 ± 2.30 with the S/O/W method. Possibly, the latter method prevented HGNS in the internal aqueous phase from diffusing to the external aqueous phase. The diameters of the microspheres ranged from 17.02 to 30.33 μm, with average diameters of 23.02 ± 6.00 and 25.23 ± 5.10 μm for microspheres generated using the W/O/W and S/O/W methods, respectively. Both types of microspheres were suitable for intramuscular injection.

### 3.3. Photothermal effects of HGNS and microspheres

Continuous exposure to NIR laser irradiation led to a relatively rapid increase in the temperature of a liquid suspension of HGNS and PRX/HGNS MS (Fig. 3a). This suspension reached a maximum temperature of 63.63 ± 0.25 °C at a higher HGNS concentration of $5.25 \times 10^{10}$ particles/mL, compared to a maximum of 54.53 ± 0.25 °C at a lower HGNS concentration ($5.25 \times 10^9$ particles/mL). By comparison, the maximum temperature of 50.60 ± 0.17 °C in a solution containing $5.25 \times 10^9$ PRX/HGNS MS was attributed to the photothermal effect of HGNS. These changes in microsphere temperature are depicted in FLIR images (Fig. 3b). In contrast, no significant change in temperature was detected when PBS (pH 7.4, 10 mM) was exposed to NIR light.

### 3.4. DSC of microspheres

The DSC thermograms (Fig. 4) revealed that PRX and PLGA exhibited endothermal peaks at 142.77 °C and 49.92 °C, respectively. The DSC thermogram for PRX/HGNS MS showed an obvious endothermic peak related to PLGA, indicating the near-complete encapsulation of PRX in the polymer.

### 3.5. NIR light-triggered release of PRX from microspheres in vitro

The PRX release profiles from microspheres exposed to NIR laser irradiation at 2 h intervals were measured *in vitro* under conditions with variable time periods, powers, polymers and preparation methods (Fig. 5). NIR irradiation led to a rapid increase in the release of PRX from PRX/HGNS MS in PBS (5 mg/mL), and which slowed when the NIR laser was powered off. Subsequently, suspensions of PRX/HGNS MS prepared via different methods were repeatedly irradiated with NIR light at a power of 2 W (5 min each time separated by 2 h intervals) (Fig. 5a). Notably, the cumulative release rate of PRX/HGNS MS prepared using the S/O/W method increased by 12.83% from the first irradiation interval (from 10.16% to 22.99%), a more rapid increase than that observed in PRX/HGNS MS prepared using the W/O/W method. The cumulative PRX release rates from PRX/HGNS MS prepared using the S/O/W method were 8.48%, 6.89% and 5.74% for the second, third and fourth NIR light radiation intervals, respectively.

Suspensions of PRX/HGNS MS were irradiated repeatedly using a NIR laser at 2 W for different exposure times (Fig. 5b). After the first 8 min irradiation, the cumulative release rate increased by 14.07% (from 10.63% to 24.70%), which differed significantly from both the increase of < 1% observed in the absence of irradiation and from the cumulative release rates of the second, third and fourth NIR light irradiation intervals. In other words, the release of PRX in response to NIR irradiation increased with increasing irradiation time. Suspensions of PRX/HGNS MS were also irradiated repeatedly with a NIR laser at different powers for a period of 5 min (Fig. 5c). After the first 5 min irradiation at 2.5 W, the cumulative release rate increased by 14.12% (from 10.54% to 24.66%), which differed significantly from both the increase of < 1% observed in the absence of irradiation and the cumulative release rates of the second, third and fourth NIR light radiation intervals. In other words, the release of PRX in response to NIR exposure increased with increasing power. Moreover, the speed of release from PRX/HGNS MS decreased as the viscosity of PLGA increased (Fig. 5d).

Furthermore, the PRX release behaviors of microspheres treated with a NIR laser at 1, 2, 4 and 6 d were measured *in vitro* under the conditions of different times, powers, polymers and preparation methods, and these analyses yielded similar conclusions (Fig. 6). NIR irradiation led to a rapid increase in PRX release from PRX/HGNS MS in PBS (5 mg/mL), compared to the condition without irradiation. Under repeated NIR laser irradiation at a power of 2 W and 5 min, PRX/HGNS MS prepared using the S/O/W method exhibited a more rapid release of PRX, compared to microspheres prepared using the W/O/W method (Fig. 6a). Furthermore, the release of PRX increased both as the irradiation time (Fig. 6b) and the power increased (Fig. 6c), whereas the drug release slowed as the viscosity of PLGA increased (Fig. 6d).

### 3.6. Cytotoxicity assessment

C2C12 myotubes, RAW macrophages, PC12 model neurons and 3T3 fibroblasts were used to evaluate the cytotoxicity of HGNS and microspheres (Fig. 7). A cytotoxicity assessment revealed no statistically significant differences between the viabilities of cells treated with various concentrations of HGNS (0.01–0.5 mg/mL) or microspheres (0.0002–0.2 mg/mL), compared with the negative control group. Simultaneously, no statistically significant differences were observed between cells treated with HGNS (0.01–0.5 mg/mL) and microspheres (0.0002–0.2 mg/mL) and exposed or not to NIR irradiation. These results indicate that the HGNS and microspheres produced using either of the indicated methods were not toxic to the model cell lines could potentially be used in biomedical applications.

### 3.7. Pharmacokinetics study

The release behaviors of different types of optimized PRX microspheres were also evaluated *in vivo* in rat models, using the mean plasma concentration-time profiles over a 2-week period (Fig. 8). The mean values of the main pharmacokinetic parameters were calculated from the pharmacokinetic data of each group using DAS 3.0 software (Drug and Statistics Software, Mathematical Pharmacology Professional Committee of China, Shanghai, China) (Table 3). The plasma concentration profiles revealed that PRX/HGNS MS prepared using the S/O/W method with NIR exhibited a release duration exceeding 2 weeks, although the peak plasma concentration, $C_{max}$, was reached at 48 ± 0.25 h after the microsphere suspension was administered intramuscularly. Compared with the other groups, optimized microspheres prepared using the S/O/W method also yielded higher values for $AUC_{0\text{-}t}$ (2229.59 ± 261.16 ng h mL$^{-1}$), $AUC_{0\text{-}\infty}$ (2482.04 ± 415.30 ng h mL$^{-1}$), $C_{max}$ (19.06 ± 4.73 ng/mL), $T_{max}$ (48.00 ± 0.25 h) and $MRT_{0\text{-}t}$ (112.91 ± 15.67 h).

When rats treated with PRX MS, PRX could be released from the PLGA microspheres *in vivo* at a very slow rate because of diffusion through the polymer matrix, water-mediated transport processes, polymer hydrolysis and erosion of biodegradable PLGA. When rats treated with PRX/HGNS MS by S/O/W, the plasma concentration of PRX increased significantly on day 1 ($p < 0.05$) and day 2 ($p < 0.01$) compared to PRX MS group. And the plasma concentration of PRX/HGNS MS by S/O/W increased significantly on day 6 ($p < 0.05$) compared to PRX/HGNS MS by W/O/W. The plasma concentration of PRX/HGNS MS by W/O/W showed no significant difference compared to PRX MS group.

### 3.8. Pharmacodynamics study

Nearly all mice treated with microspheres exhibited an upward trend in weight (data were not shown). During the rotarod test, the latency decreased significantly after an intraperitoneal injection of MPTP ($p < 0.001$), indicating the successful generation of a PD model (Fig. 9a). In the model group, no significant difference in latency was observed after the intramuscular injection of physiological saline or microspheres. However, the three experimental groups exhibited increases in latency. Mice treated with PRX/HGNS MS without NIR exhibited a significant difference in latency relative to the model group after 3 days, which was characterized by a slow increase ($p < 0.001$). This slow recovery is mainly due to the biodegradability of PLGA including diffusion through the polymer matrix, water-mediated transport processes, polymer hydrolysis and erosion. Mice treated with PRX/HGNS MS prepared using the W/O/W or S/O/W method and exposed to NIR irradiation exhibited significant differences in latency over time when compared with the model group ($p < 0.001$). Notably, more rapid recovery was observed in mice receiving microspheres prepared using S/O/W because of photothermal effect. In all mice treated with PRX/HGNS MS (regardless of preparation method) and NIR irradiation exhibited more rapid recovery on days 1, 2, 4 and 6.

At 14 days after the intramuscular injection, the model mice (66.00 ± 37.18 s) still exhibited a significant decrease in the fall latency, compared with the control group ($p < 0.001$) (Fig. 9b). However, the latency times of mice treated with PRX/HGNS MS prepared using W/O/W and S/O/W with NIR were extended to 247.50 ± 15.18 s ($p < 0.01$) and 291.17 ± 8.66 s ($p < 0.001$), and these increases in latency were observed significantly more rapidly than without NIR irradiation because of photothermal effect.

The ELISA analysis of homogenized striatum samples revealed that

the respective levels of DA, HVA and DOPAC in the model group samples, 4.13 ± 0.96, 1.93 ± 0.43 and 8.97 ± 1.49 ng/mg tissue, were significantly lower than those in the control group (7.79 ± 1.03, 3.56 ± 0.74 and 12.96 ± 1.40 ng/mg, respectively) ($p < 0.001$) (Fig. 9c). However, the concentrations of DA, HVA and DOPAC gradually recovered following microsphere administration in the three experimental groups. Mice treated with PRX/HGNS MS prepared using the S/O/W exhibited significant recoveries of DA (7.14 ± 1.19 ng/mg tissue) ($p < 0.01$), HVA (3.59 ± 0.51 ng/mg tissue) ($p < 0.01$) and DOPAC (13.43 ± 1.62 ng/mg tissue) ($p < 0.05$) compared to the group without NIR irradiation. Nevertheless, mice treated with PRX/HGNS MS prepared using the W/O/W exhibited no significant compared to the group without NIR irradiation.

### 3.9. Immunohistochemistry

TH, a rate-limiting enzyme in the DA synthesis pathway, is a biomarker of dopaminergic neurons. The immunohistochemical results showed that a greater optical density of TH in the striatum slides was associated with stronger positive expression (Fig. 10a). $TH^+$ showed brownish-yellow staining in the slides, and the darker of brownish yellow, the higher levels of $TH^+$. In the model group, the striatum $TH^+$ optical density decreased to 2.08 ± 0.51, compared with 8.62 ± 0.97 in the control group ($p < 0.001$). And this indicated successful modeling. However, treatment with PRX/HGNS MS by W/O/W (3.19 ± 0.58, $p < 0.05$) and S/O/W (4.76 ± 0.64, $p < 0.001$) method significantly reduced the losses of TH in the striatum, compared with the group without NIR irradiation. In addition, mice treatment with PRX/HGNS MS without NIR (2.33 ± 0.47) recovered slowly that may be due to TH-expressing interneurons was just one of the striatal neurons [22,23]. In a representative image of a striatal section, TH is indicated by brownish-yellow staining (blue nuclei indicate hematoxylin counterstaining) (Fig. 10b). The demonstrated staining reveals a severe loss of dopaminergic neurons after MPTP exposure. By contrast, treatment with PRX/HGNS MS, especially those prepared using S/O/W, protected the neurons from MPTP-induced damage.

## 4. Conclusions

Here, we fabricated PRX/HGNS MS using a S/O/W emulsion-solvent evaporation method and demonstrated the ability of these microspheres to enable modulated drug release in response to NIR exposure, compared to non-responsive microspheres. In comparison with microspheres prepared using the W/O/W method, PRX/HGNS MS prepared using the S/O/W method exhibited a stronger photothermal effect which enabled the repeated achievement of controllable, rapid drug release in response to NIR laser irradiation both *in vitro* and *in vivo*. No significant differences in cytotoxicity were observed with HGNS and PRX/HGNS MS, compared to negative controls. Pharmacodynamics and immunohistochemistry studies demonstrated that rodents treated with PRX/HGNS MS prepared using the S/O/W method and exposed to NIR irradiation recovered more rapidly from MPTP-induced damage because of the more rapid and enhanced drug release.

PRX/HGNS MS using S/O/W method were administrated once every two weeks and could be controlled to release drugs quickly at a certain moment. Compared to the existing oral pramipexole of three times a day, patients can get higher plasma concentration at the moment only by a NIR laser button conveniently when they suffer from a sudden onset like cognitive impairment, tremor, rigidity and bradykinesia. The results clearly demonstrate that this NIR light-responsive drug delivery system could be applied to the special diseases, including PD, and would thus address patients' mobility problems in a smart, controllable and remotely triggerable manner. In the future, this NIR light-responsive drug delivery system can be used to treat more diseases that makes patients' cognitive or mobility abilities poor in clinical applications.

## Acknowledgment

Supported by the Central Lab of General Biology, Jilin University, China.

## References

[1] J. Motyl, L. Przykaza, P.M. Boguszewski, P. Kosson, J.B. Strosznajder, Pramipexole and Fingolimod exert neuroprotection in a mouse model of Parkinson's disease by activation of sphingosine kinase 1 and Akt kinase, Neuropharmacology 135 (2018) 139–150.
[2] D.R. Kalaria, P. Patel, V. Merino, V.B. Patravale, Y.N. Kalia, Controlled iontophoretic delivery of pramipexole: electrotransport kinetics in vitro and in vivo, Eur. J. Pharm. Biopharm. 88 (2014) 56–63.
[3] Y.Z. Wang, X.F. Yu, P. Zhang, Y.L. Ma, L. Wang, H.L. Xu, D.Y. Sui, Neuroprotective effects of pramipexole transdermal patch in the MPTP-induced mouse model of Parkinson's disease, J. Pharmacol. Sci. 138 (2018) 31–37.
[4] A. Chierchia, N. Chirico, L. Boeri, I. Raimondi, G.A. Riva, M.T. Raimondi, M. Tunesi, G. Giordano, G. Forloni, Secretome released from hydrogel-embedded adipose mesenchymal stem cells protects against the Parkinson's disease related toxin 6-hydroxydopamine, Eur. J. Pharm. Biopharm. 121 (2017) 113–120.
[5] D.R. Kalaria, M. Singhal, V. Patravale, V. Merino, Y.N. Kalia, Simultaneous controlled iontophoretic delivery of pramipexole and rasagiline in vitro and in vivo: transdermal polypharmacy to treat Parkinson's disease, Eur. J. Pharm. Biopharm. 127 (2018) 204–212.
[6] H.J. Urbieta, B. Gago, A.Q. Varela, T.R. Chinchilla, L.M. Galán, A. Oregi, A.B. Iguerategui, M.D. Alvarado, I.N. Gómez, C. Marin, P.O. Fernagut, M.R. Oroz, Pramipexole-induced impulsivity in mildparkinsonian rats: a model of impulse control disorders in Parkinson's disease, Neurobiol. Aging 75 (2018) 126–135.
[7] S.H. Fox, R. Katzenschlager, S.Y. Lim, B. Barton, M.A. Rob, K. Seppi, M. Coelho, C. Sampaio, International Parkinson and movement disorder society evidence-based medicine review: update on treatments for the motor symptoms of Parkinson's disease, Mov. Disord. 33 (2018) 1248–1266.
[8] R. Raj, S. Wairkar, V. Sridhar, R. Gaud, Pramipexole dihydrochloride loaded chitosan nanoparticles for nose to brain delivery: development, characterization and in vivo anti-Parkinson activity, Int. J. Biol. Macromol. 109 (2018) 27–35.
[9] S. Loiodice, P. McGhan, V. Gryshkova, R. Fleurance, D. Dardou, A. Hafidi, A.N. Costa, F. Durif, Striatal changes underlie MPEP-mediated suppression of the acquisition and expression of pramipexole-induced place preference in an alpha-synuclein rat model of Parkinson's disease, J. Psychopharmacol. 31 (2017) 1323–1333.
[10] B.P. Timko, T. Dvir, D.S. Kohane, Remotely triggerable drug delivery systems, Adv. Mater. 22 (2010) 4925–4943.
[11] H.J. Cho, M. Chung, M.S. Shim, Engineered photo-responsive materials for near-infrared-triggered drug delivery, J. Ind. Eng. 31 (2015) 15–25.
[12] A. Saneja, R. Kumar, D. Arora, S. Kumar, A.K. Panda, S. Jaglan, Recent advances in near-infrared light-responsive nanocarriers for cancer therapy, Drug Discov. Today 23 (2018) 1115–1125.
[13] K.R. Deng, C.X. Li, S.S. Huang, B.G. Xing, D.Y. Jin, Q.G. Zeng, Z.Y. Hou, J. Lin, Recent progress in near infrared light triggered photodynamic therapy, Small 13 (2017).
[14] S. Adams, J.Z. Zhang, Unique optical properties and applications of hollow gold nanospheres (HGNs), Coordination Chem. Rev. 320–321 (2016) 18–37.
[15] Q.Q. Ren, L.Y. Bai, X.S. Zhang, Z.Y. Ma, B. Liu, Y.D. Zhao, Y.C. Cao, Preparation, modification, and application of hollow gold nanospheres, J. Nanomater. 2015 (2015) 1–7.
[16] C.H. Chen, J.B. Yang, H.B. Han, J.W. Chen, Y.D. Wang, Q.S. Li, Y.B. Wang, Disulfiram-loaded porous PLGA microparticle for inhibiting the proliferation and migration of non-small-cell lung cancer, Int. J. Nanomed. 12 (2017) 827–837.
[17] Z.X. Su, Y.N. Shi, L.S. Teng, X. Li, L.X. Wang, Q.F. Meng, L.R. Teng, Youxin Li, Biodegradable poly(D, L-lactide-co-glycolide) (PLGA) microspheres for sustained release of risperidone: Zero-order release formulation, Pharm. Dev. Technol. 1 (6) (2011) 377–384.
[18] J. You, R.P. Shao, X. Wei, S.J. Gupta, C. Li, Near-infrared light triggers release of Paclitaxel from biodegradable microspheres: photothermal effect and enhanced antitumor activity, Small 6 (2010) 1022–1031.
[19] Y.C. Pu, F. Song, W.C. Zhang, S. Lindley, S. Adams, J.J. Zhang, Size-tunable synthesis of hollow gold nanospheres through control of reaction temperature, Part. Part. Syst. Char. 34 (2017) 1–8.
[20] P.F. Sandra, D.C. Wang, D.A. Wheeler, R. Newhouse, J.K. Hensel, A. Schwartzberg, L.H. Wang, J.J. Zhu, M.B. Flores, J.Z. Zhang, Highly reproducible synthesis of hollow gold nanospheres with near infrared surface plasmon absorption using PVP as stabilizing agent, J. Mater. Chem. 21 (2011) 2344–2350.
[21] Y.Y. Lau, G.D. Hanson, N. Ichhpurani, Determination of pramipexole (U-98,528) in human plasma and urine by high-performance liquid chromatography with electrochemical and ultraviolet detection, J. Chromatography B. 683 (1996) 217–223.
[22] F.F. Geibl, M.T. Henrich, W.H. Oertel, Mesencephalic and extramesencephalic dopaminergic systems in Parkinson's disease, J. Neural. Transm. (Vienna) 126 (2019) 377–396.
[23] T. Nagatsu, A. Nakashima, H. Ichinose, K. Kobayashi, Human tyrosine hydroxylase in Parkinson's disease and in related disorders, J. Neural. Transm. (Vienna) 126 (2019) 397–409.